Estuaries and Coasts (2022) 45:1861–1878
https://doi.org/10.1007/s12237-022-01081-x

MANAGEMENT APPLICATIONS

# Development and Application of Landsat-Based Wetland Vegetation Cover and UnVegetated-Vegetated Marsh Ratio (UVVR) for the Conterminous United States

**Neil K. Ganju[1] · Brady R. Couvillion[2] · Zafer Defne[1] · Katherine V. Ackerman[1]**

Received: 14 January 2022 / Revised: 6 April 2022 / Accepted: 6 April 2022 / Published online: 2 May 2022


**Abstract**
Effective management and restoration of salt marshes and other vegetated intertidal habitats require objective and spatially integrated metrics of geomorphic status and vulnerability. The unvegetated-vegetated marsh ratio (UVVR), a recently developed metric, can be used to establish present-day vegetative cover, identify stability thresholds, and quantify vulnerability to open-water conversion over a range of spatial scales. We developed a Landsat-based approach to quantify the within-pixel vegetated fraction and UVVR for coastal wetlands of the conterminous United States, at 30-m resolution for 2014–2018. Here we present the methodology used to generate the UVVR from spectral indices, along with calibration, validation, and spatial autocorrelation assessments. We then demonstrate multiple applications of the data across varying spatial scales: first, we aggregate the UVVR across individual states and estuaries to quantify total vegetated wetland area for the nation. On the state level, Louisiana and Florida account for over 50% of the nation's total, while on the estuarine level, the Chesapeake Bay Estuary and selected Louisiana coastal areas each account for over 6% of the nation's total vegetated wetland area. Second, we present cases where this dataset can be used to track wetland change (e.g., expansion due to restoration and loss due to stressors). Lastly, we propose a classification methodology that delineates areas vulnerable to open-water expansion based on the 5-year mean and standard deviation of the UVVR. Calculating the UVVR for the period-of-record back to 1985, as well as regular updating, will fill a critical gap for tracking national status of salt marshes and other vegetated habitats through time and space.

**Keywords** Remote-sensing · Salt marshes · Tidal wetlands · Vulnerability · Geomorphology

## Introduction

Coastal wetlands, including salt marshes, mangroves, and other vegetated intertidal habitats, provide numerous ecosystem services (Barbier et al. 2011). These habitats are also increasingly threatened by sea-level rise, eutrophication, sediment deficits, storms, and anthropogenic development (Leonardi et al. 2018; Kirwan et al. 2010; Deegan et al. 2012). Though field-based assessments have linked wetland vulnerability to these processes over limited spatial scales (Cahoon et al. 2019), coastal managers and researchers could benefit from spatially comprehensive metrics that integrate a myriad of processes.

The concept of vegetative cover as a stability metric is established (Neckles et al. 2013); however, prior studies have been based on point, quadrat, or transect scales. A wealth of literature has reinforced that wetlands are three-dimensional biogeomorphic structures (Redfield 1972; Fagherazzi 2013; Mariotti 2020) and therefore a complete spatial characterization of vegetation is necessary. Prior efforts have used remote sensing and aerial imagery to track salt marsh dieback (Rangoonwala et al. 2016; Burns et al. 2021), characterize gross primary production (Feagin et al. 2020), and evaluate large-scale coastal land loss (Couvillion et al. 2017). In this study, we extend the use of remote sensing by generating a conterminous United

Communicated by Richard C. Zimmerman

✉ Neil K. Ganju
nganju@usgs.gov

[1] U.S. Geological Survey, Woods Hole Coastal and Marine Science Center, 384 Woods Hole Road, Woods Hole, MA 02543, USA

[2] Livestock Show Office, U.S. Geological Survey, Wetland and Aquatic Research Center, Baton Rouge, LA 70803, USA

States (CONUS)-wide dataset of the vegetated fraction and unvegetated-vegetated marsh ratio.

The unvegetated-vegetated marsh ratio (UVVR) is a spatially integrative metric that correlates with sediment budgets and sea-level rise (Ganju et al. 2017); it is defined as:

$$UVVR = A_{uv}/A_v \quad (1)$$

where $A_{uv}$ is the unvegetated area within a specified domain, and $A_v$ is the vegetated area. The total area of the wetland domain, $A_d$, is the sum of $A_{uv}$ and $A_v$ and the vegetated fraction, $F_v$, is therefore:

$$F_v = A_v/A_d \quad (2)$$

Unvegetated areas can represent bare sediment, pools, channels, and intertidal flats. Vegetated areas are typically wetland plain areas, and in a "binary" context, any vegetated plain, regardless of stem density, would be considered vegetated at some nominal spatial scale (based on sampling resolution and methodology, discussed in the "Resolution and Aggregation Scales" section). In this study, we quantified the vegetated fraction, $F_v$, which is related to the UVVR through:

$$UVVR = \left(1/F_v\right) - 1 \quad (3)$$

Note that the UVVR is a unitless ratio derived from the vegetated fraction and is therefore not suitable for calculating averages ($F_v$ should be used for averages and aggregates, and then converted to UVVR).

The UVVR was originally developed in conjunction with field-based sediment transport measurements over individual marsh complexes, and then expanded across entire estuaries following a "marsh unit" concept akin to a hydrologic watershed (Defne et al. 2020; Ganju et al. 2020). The metric captures the tendency of vulnerable wetland areas to convert to open water in response to some external forcing, whether it is episodic dieback from salinity stress, gradual loss to sea-level rise, or lateral erosion from wave attack. The UVVR ranges from 0 (fully vegetated) to near infinity for nearly unvegetated areas (completely open water is technically an undefined number), but all sites studied by Ganju et al. (2017) were below 1, with the most unstable wetland complex (Blackwater National Wildlife Refuge region, Maryland, USA) having a value of 0.94. Ganju et al. (2017), as well as other independent investigations (Wasson et al. 2019; D'Alpaos and Marani 2016), have shown a stability threshold in the range of 0.10–0.15. Above a UVVR of 1, a marsh complex may cease to be geomorphically characterized as a vegetated wetland and may function more as an estuary; therefore, the utility of the UVVR as a predictive metric diminishes above this threshold. The vegetated fraction metric, $F_v$, on the other hand, is a basic quantity that identifies the change in inventory in response to restoration and loss.

The UVVR, by definition, is calculated over an areal basis, either across hydrologically distinct marsh units or as a raster/pixel-based metric; this distinguishes it from traditional metrics such as percent cover which are applied on quadrat or transect scales. Both the marsh unit and pixel approaches are valuable depending on the application. Prior work (Defne et al. 2020; Ganju et al. 2020) implemented detailed marsh-unit mapping, using elevation and watershed delineation tools, to compute the UVVR and other important metrics at scales that are often used by coastal managers (i.e., marsh parcels separated by channels or other geomorphic features). Satellite-based, pixel-level methods can be used to characterize broader spatial areas and relate vulnerability to spatially varying external forces such as sea-level rise, sediment supply, and tidal range (Sun et al. 2018). They are also valuable for rapid comparisons of stable and vulnerable areas and for the generation of baseline metrics over areas that may be subject to restoration or intervention in the future. In this study, we present the development and application of a national UVVR dataset using Landsat 8 satellite imagery (Vermote et al. 2016). We first describe the methodology and assess the derived UVVR in comparison with high-resolution imagery and classified data. We then demonstrate the use of the UVVR in evaluating state- and estuary-level wetland cover, and present potential uses of the data in tracking restoration, dieback, and relative vulnerability.

## Methods

Here we describe the analysis of spectral Landsat imagery to first calculate within-pixel vegetated fractional cover estimates, and then the within-pixel UVVR. We calibrate and validate the analysis with spectral Sentinel-2 satellite imagery (10-m resolution; ESA 2022), and US Department of Agriculture's National Agricultural Inventory Program (NAIP; U.S. Department of Agriculture 2022) aerial imagery (~ 1-m resolution). Additionally, we compare the Landsat fractional cover estimates with an unsupervised classification of NAIP imagery in two ways: (1) by aggregating binary (vegetated or unvegetated) classified NAIP pixels to Landsat pixels and (2) calculating the aggregates from Landsat fractional cover estimates and classified NAIP pixels for predetermined marsh units. These workflow steps are presented in Fig. 1.

### Satellite Imagery Processing and Calibration for Annual Data

For this application, we considered the conterminous United States along all coastal regions landward to an elevation

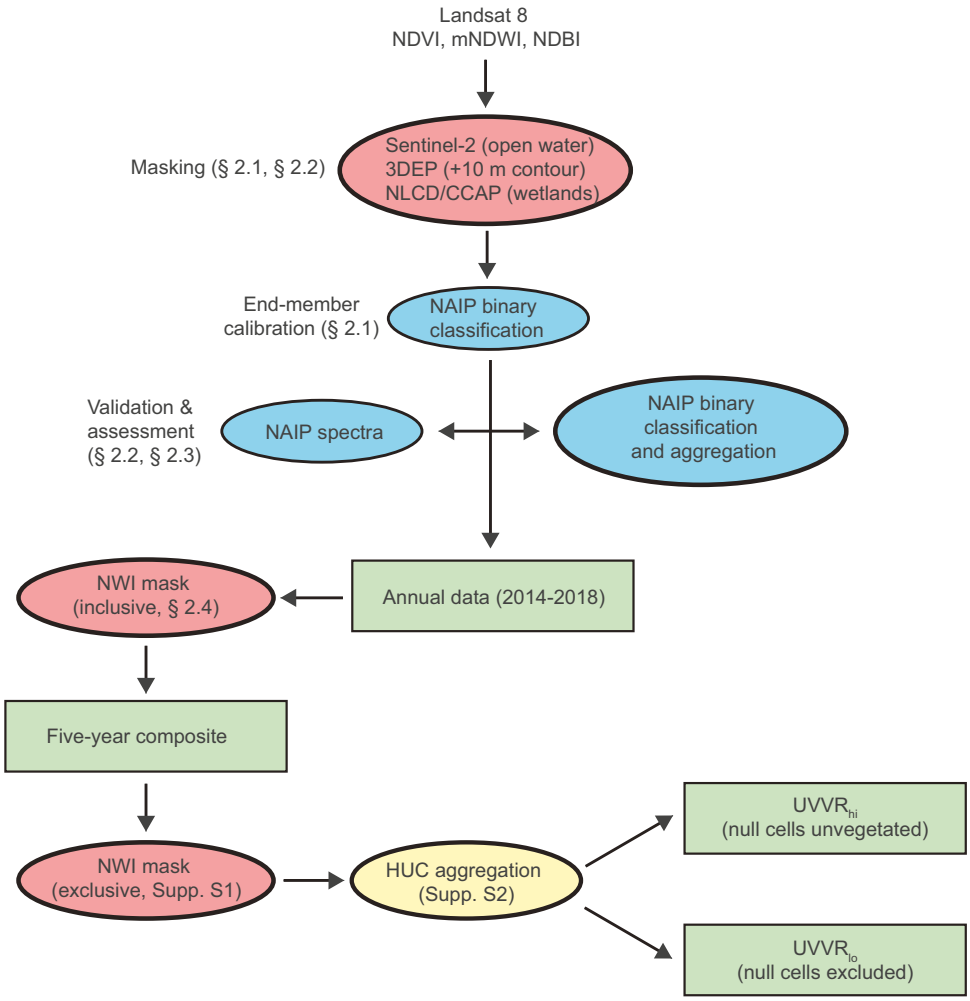


**Fig. 1** Processing workflow for vegetated fraction and UVVR from Landsat imagery. Pink ellipses represent masking steps, blue ellipses represent calibration, validation, and assessment steps, yellow ellipse represents aggregation step, and green boxes represent outputs

of + 10 m NAVD88 (U.S. Geological Survey 2022a) and seaward to the federal waters boundary (Fig. 2). The National Land Cover Dataset (Wickham et al. 2021) and Coastal Change Analysis Program (National Oceanic and Atmospheric Administration 2022) dataset were used to identify wetland areas and mask the final output. While satellites such as Sentinel and other commercial satellites have a higher spatial resolution, Landsat imagery was selected for use because of its 45-year long period of record. Landsat 8 (2013–present) was used for this assessment (Vermote et al. 2016). Below, we briefly describe the methodology and assessment; further details can be found in Couvillion et al. (2021).

We grouped cloud-free images for each year and used the annual median value of each index at each pixel for each year for this analysis. Masking, using the *Pixel_QA* band available in Landsat 8 imagery, was first used to remove clouds, cloud shadows, and other potential sources of image contamination (e.g., saturation) in the individual dates of imagery (U.S. Geological Survey 2022b). An annual median was calculated from the remaining observations. A median was used due to lower sensitivity than the mean to sources of contamination unrecognized by the previously mentioned mask.

The following indices were calculated for each image in the collection:

$$mNDWI = (G - SWIR)/(G + SWIR) \quad (4)$$

$$NDVI = (NIR - R)/(NIR + R) \quad (5)$$

$$NDBI = (SWIR - NIR)/(SWIR + NIR) \quad (6)$$

where *mNDWI* is the modified Normalized Difference Water Index (Xu 2006), *NDVI* is the Normalized Difference Vegetation Index (Kriegler et al. 1969), *NDBI* is the Normalized Difference Built-up Index (Zha et al. 2003), and *R*, *G*, *SWIR*, and *NIR* are the red, green, shortwave infrared, and near-infrared bands, respectively.

Linear spectral unmixing was used to determine the relative abundance of the targets of interest (i.e., vegetated and unvegetated fractions) in the annual median images created in the previous step. Linear spectral unmixing assumes that the reflectance of each pixel is a linear combination of the reflectance of each target present within the pixel. Linear spectral unmixing requires the designation of

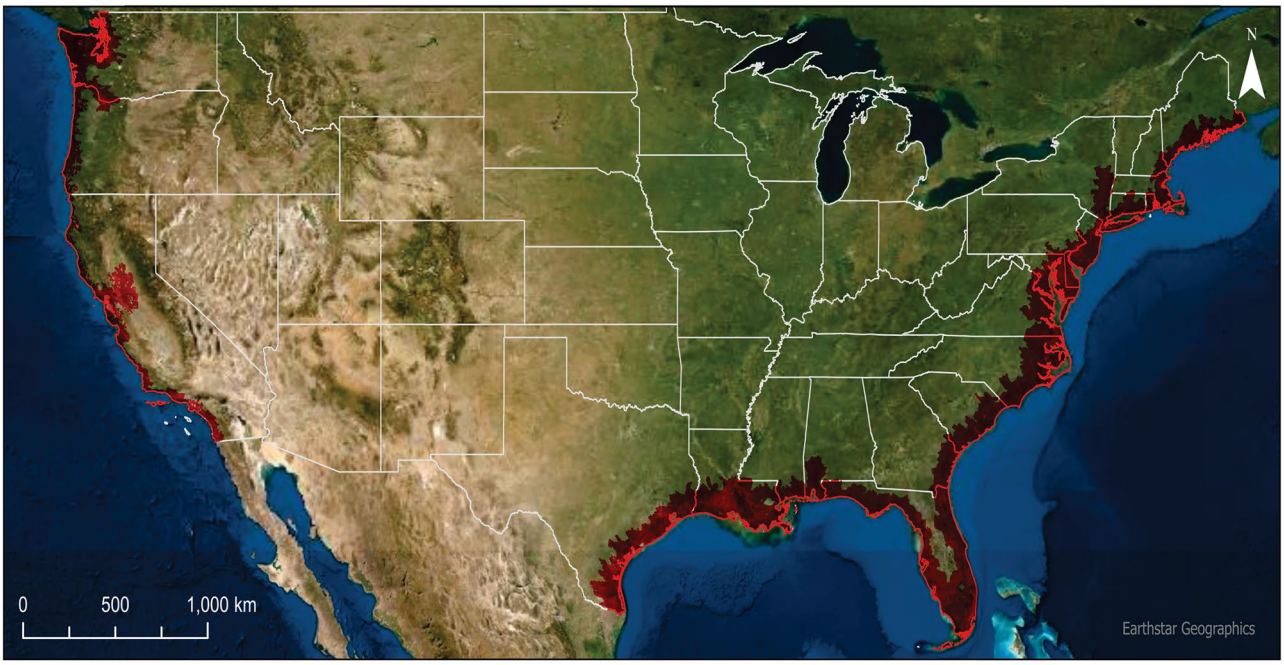


**Fig. 2** Domain (shown in red) considered for Landsat 8-derived UVVR coverage for the conterminous USA. This domain includes wetland areas from the seaward boundaries of federal waters, landward to the 10-m contour relative to the North American Vertical Datum of 1988. Background map from Earthstar Geographics

"endmembers," or pixel values which represent a homogenous target of each class.

High-resolution aerial-imagery based (NAIP) analyses of three large estuary-marsh complexes (Ganju et al. 2020) were used to develop endmembers in Landsat 8 data which represented unvegetated (bare earth), vegetated, and water conditions (Couvillion et al. 2018). These products yielded binary classifications of each pixel and were aggregated from a ~ 1-m spatial resolution to 30-m spatial resolution to match the Landsat pixels and the percent unvegetated/vegetated/water in each 30-m pixel was recorded. These data were binned into 1% intervals from 1 to 99% of each category. Bins for 0% and 100% were not used as these categories often contained variability not indicative of the fractions of the targets of interest.

Mean values of the Landsat-based *NDVI*, *mNDWI*, and *NDBI* for time periods which best matched the calibration datasets were recorded in each interval. Endmember values were calculated from the intercepts at 0 and 100% of the line which best fit the calibration data. The pixel values of the resulting images indicated the fraction of the pixel comprised by that target or endmember.

The Landsat orbit allows for a return interval of 16 days at a given location, yielding ~ 23 images per year at a given location (not considering cloud interference). This therefore prevents tidal aliasing (i.e., return interval is not aligned with semi-diurnal, diurnal, or spring-neap cycle) and yields enough images within a year to capture a mixture of high and low water events. Compositing of annual data over 5 years (the "Multi-year Composite for Coastal Wetlands" section) further minimizes potential artifacts due to tides.

## Validation and Assessment with Higher-Resolution Spectral Data

We assessed the moderate resolution spectral unmixing estimate with higher-resolution data to determine if the 30-m satellite product captures the same vegetation coverage as a finer-resolution aerial product. The datasets used for validation were created from high-resolution (~ 1 m) datasets representing median conditions during the 2014–2019 time period. We used imagery from the US Department of Agriculture's National Agricultural Inventory Program (NAIP), as well as Sentinel-2 satellite imagery in consistently open-water areas, to estimate the fractional composition of unvegetated, vegetated, and water in each pixel. Sentinel-2 imagery was used to identify persistent open water and reduce the error in these areas often caused by issues such as inconsistency in spectral reflectance values in NAIP data. Random samples from these higher-resolution datasets were used to assess the 30-m resolution Landsat datasets. To facilitate comparability with the Landsat datasets, the finer resolution data were aggregated to a 30-m spatial resolution.

Landsat-derived unvegetated, vegetated, and water fractional cover estimates for the same 2014–2019 period were reclassified into 1% interval bins and a stratified random sample was taken from each bin from 1 to 99%. For the purposes of this analysis, 0% and 100% cover were excluded from this random sample, as we are most concerned with fractional estimates of cover. In general, 100% water is straightforward to quantify from a spectral perspective, and the inclusion of large areas of 100% water (for example) would bias the statistics towards higher accuracy. The sampling consisted of 500,000 random points which were intersected with the corresponding vegetated, unvegetated, or water percent derived from the NAIP images composited over the same time-period. For the purposes of this accuracy assessment, the NAIP-derived fractional cover estimates were considered the reference data and compared to the Landsat-derived estimates. The root mean squared error (RMSE) and bias of the Landsat-derived fractional cover estimates were calculated.

## Validation and Assessment with Aerial Imagery-Based Classification

Visual classification methods for evaluating vegetated and unvegetated (bare land and water) area were also compared with the Landsat-derived method for determining fractional estimates. For this comparison, we used an additional data set for the wetlands on the eastern side of Chesapeake Bay (Ackerman et al. 2021). These data were generated in the same fashion as the calibration data used in the "Satellite Imagery Processing and Calibration for Annual Data" section (Ganju et al. 2020). In brief, an unsupervised classification of NAIP four-band imagery and elevation data was used to identify 32 imagery classes. The user then identified each class as either unvegetated or vegetated. The final result of this process is a binary classification of vegetated or unvegetated pixels. Two methods using the 0.60-m spatial resolution 2018 NAIP imagery were compared with the Landsat classification: the first method aggregated binary pixels across delineated marsh units (Ganju et al. 2020) to compute a NAIP-based fractional vegetative cover. The Landsat-based 30-m pixels (and their associated fractional vegetation cover value) were then aggregated over those same units. For the NAIP imagery, we calculated the vegetated fraction of the marsh unit by first dissolving the unvegetated and vegetated areas smaller than nine pixels (to eliminate spurious pixels; this yields a minimum mapping unit of nominally 3.25 $m^2$ for 0.60 m resolution imagery) into the surrounding vegetated and unvegetated regions, respectively, and then calculating the vegetated area in each marsh unit (Ackerman et al. 2021). For the Landsat imagery, we used the vegetated fraction of the 2018 Atlantic Coast Landsat UVVR raster (Couvillion et al. 2021) to generate a mean vegetated fraction for each marsh unit. There were 8,518 marsh units in this region, 130 of which did have null Landsat values due to complete open water within the pixel. The second method directly compared NAIP pixels aggregated up to the same resolution as the Landsat pixels. For this method, we first created a random sample of points within the exclusive mask (see exclusive mask description below), with a minimum distance of 60 m between points to avoid computation of adjacent pixels. We then extracted the footprint of the corresponding Landsat pixel containing the random point, aggregated the 1-m resolution NAIP pixels over that footprint, and computed the fractional vegetative cover. We also computed total vegetated area over all marsh units using both Landsat and NAIP imagery, to compare aggregated estimates.

## Multi-year Composite for Coastal Wetlands

Annual data may contain spatiotemporal variability due to fluctuating water levels, vegetation, or anthropogenic effects. Wasson et al. (2019) showed that detecting meaningful changes in vegetation cover and the UVVR with aerial imagery was feasible at the decadal level. Therefore, we provide a 5-year composite dataset for long-term tracking of vegetation changes. For the composite product, we defined a mask that further limited the spatial coverage to tidal areas, coastal vegetation, and adjacent coastal lands, based on the National Wetland Inventory (NWI) delineation of coastal wetlands (Cowardin et al. 1979). For analysis purposes, we used a more restrictive mask that included all estuarine intertidal subsystems, and all subsystems in the classification that were marked with a saline or freshwater tidal modifier (U.S. Fish and Wildlife Service 2022a). Emergent vegetation and unconsolidated shore classes from the tidal riverine classification were also included. All nontidal subclasses or unconsolidated shore marked with special modifiers (farmed, artificial, excavated, etc.) from lacustrine and palustrine systems was excluded (see Couvillion et al. 2021 metadata for detailed listing of subclasses that were included and excluded). Using the annual data, we calculated a 5-year mean value of the vegetated fraction and its standard deviation for each pixel. The standard deviation is presented as the potential uncertainty in the 5-year mean value, and the standard deviation of the UVVR is used later as a threshold for detecting vulnerability. Note that in practice, spatial and temporal averages should be computed from the vegetated fraction then converted to UVVR following Eq. (3) as the UVVR is a unitless ratio. The aforementioned mask is then applied to the 5-year mean and standard deviation.

## Assessing the Robustness of Spatial Patterns

Temporal variability and therefore uncertainty in the UVVR at a given pixel can be simply addressed using the standard deviation in UVVR at each pixel through time. This is

predicated on the assumption that annual variations may either be artifacts or short-term variations due to actual processes that are not representative of average wetland conditions. If we accept that assumption, then the underlying spatial patterns in the UVVR may come into question. We can address this by using spatial autocorrelation and the variogram shape to test if broad-scale patterns (despite pixel-level variability) are robust, thereby lending confidence in the relative value of the UVVR across a landscape and enabling comparison within both the annual and 5-year composite data. The variogram quantifies the spatial scale of variance and can identify inherent spatial patterns (or lack thereof) within the data. For example, if a marsh complex consists of regularly spaced ditches and marsh plain, the variance in UVVR would peak at the spacing of the ditches; conversely if the UVVR pattern consisted of random noise, the variance should be constant (and small). These patterns should be relatively consistent from year-to-year if the satellite-derived metrics contain a high signal-to-noise ratio.

We selected five individual marsh regions of varying morphology and environmental setting (Sandwich Marsh, Massachusetts; Saxis Wildlife Management Area, Virginia; Delta National Wildlife Refuge, Louisiana; Bair Island, California; and the Skagit River Delta, Washington) to assess the robustness of the spatial patterns. Uniform areas of 125 × 125 pixels (or 3.75 × 3.75 km) were selected, and the anisotropic variogram was computed with the UVVR values for each year using the MATLAB variogram function (Schwanghart 2021) and the associated default parameters (six pixel bins, half of the total distance for the maximum distance). The variance was normalized by the maximum value to simplify annual comparisons. The mean UVVR and standard deviation were also computed for visual comparison.

## Results

### Calibration

Endmember values were calculated from the line which best fit the calibration data. Initially, spectral unmixing consisted of separating land and water categories on the basis of the mNDWI. The mNDWI values of these lines at 0% land (100% water) and 100% land (0% water) were 0.15388 and −0.272949, respectively, in wetland areas.

Following unmixing into land and water categories, a second iteration of linear spectral unmixing was used to quantify the unvegetated and vegetated components of Landsat pixels. For this process, NDVI and NDBI indices were used. The values of the endmembers for those indices were 0.0713 (NDVI) and −0.0402 (NDBI) for 0% vegetated land (100% unvegetated) and 0.5575 (NDVI) and −0.1586 (NDBI) for 100% vegetated land (0% unvegetated).

### Validation and Assessment: Resolution

Using a stratified random sample of 500,000 pixels, the overall RMSE of the Landsat-derived percent unvegetated, vegetated, and water estimates (when compared to NAIP-derived estimates) were 13%, 18%, and 17%, respectively. Overall bias in the Landsat-derived percent unvegetated, vegetated, and water estimates were + 0.81%, + 1.5%, and −0.87%, respectively, as compared to the NAIP-derived datasets. This indicates that overall, the Landsat-derived product overestimates unvegetated and vegetated land, and slightly underestimates water compared to the NAIP analyses.

The overall RMSE and bias results are considerably affected by the distribution of values within the data set, which is heavily biased toward pixels containing more than 70% land. The relatively low bias at this range of the data set biases the overall statistics toward a low bias. It is important to note however that the bias and RMSE vary through the percent cover estimate range.

Overestimates of percent vegetated land were highest in the lower portions of the percent cover range (i.e., vegetated cover from ~ 1 to 33%). The Landsat-derived product overestimated percent vegetated substantially in this portion of the range (bias: + 16%). Conversely, an underestimate of water was typical in these regions. At the higher end of the range (i.e., NAIP-derived percent unvegetated and vegetated cover from ~ 70 to 100%), the Landsat-derived percent unvegetated and percent vegetated and NAIP-derived percent vegetated were in close agreement. Note that the NAIP-derived product is being designated as truth due to its superior spatial resolution; however, it also contains error. We discuss this later as a source of uncertainty when using remote-sensing methods for vegetative cover.

### Validation and Assessment: Classification

Comparison of the Landsat-derived vegetated fraction with NAIP-based classification methods was largely consistent with the Landsat-to-NAIP spectral comparison in terms of error, though bias was higher. For the marsh-unit comparison, we aggregated the vegetation fraction estimates from Landsat pixels over 8,518 marsh units in Chesapeake Bay and compared them with vegetation fraction estimates using the NAIP pixel-based classification method. The RMSE, mean absolute deviation, and median difference were 17%, 12%, and 7%, respectively. The total vegetated area using the NAIP-based classification was 314 $km^2$ (over a 356 $km^2$ total area), while the Landsat-derived fractional estimate yielded 283 $km^2$ of vegetated area over 347 $km^2$. The total areas between the two methods differ due to resolution of the Landsat pixels; if scaled to match, the vegetated area estimate from Landsat increases to 290 $km^2$, yielding a 7.6% difference between the two methods.

For the aggregated pixel comparison, we selected 12,663 random points from the Chesapeake Bay domain, extracted the corresponding Landsat pixel footprint and vegetated fraction value, and aggregated the NAIP-based binary pixels to compute a vegetation fraction. Errors were similar to the marsh-unit comparison, with RMSE, mean absolute deviation, and median differences of 19%, 13%, and 5%, respectively. In completely vegetated areas, agreement was very high, resulting in many difference values near zero for the aggregated pixel comparison (Fig. 3). As discussed in the NAIP vs. Landsat spectral indices comparison (the "Validation and Assessment: Resolution" section), Landsat-based values tended to overestimate vegetative cover in less vegetated areas but perform well in completely vegetated areas. This resulted in an overall bias (underestimation) of 5–7% as quantified above, given that 50% of the areas are more than 97% vegetated (based on aggregated NAIP pixels). It is important to note the conceptual difference between a visually classified pixel (with a binary 0 or 1 value) and a within-pixel spectral estimate that is quantifying vegetative cover over a larger footprint. We discuss nuances regarding binary classifications and

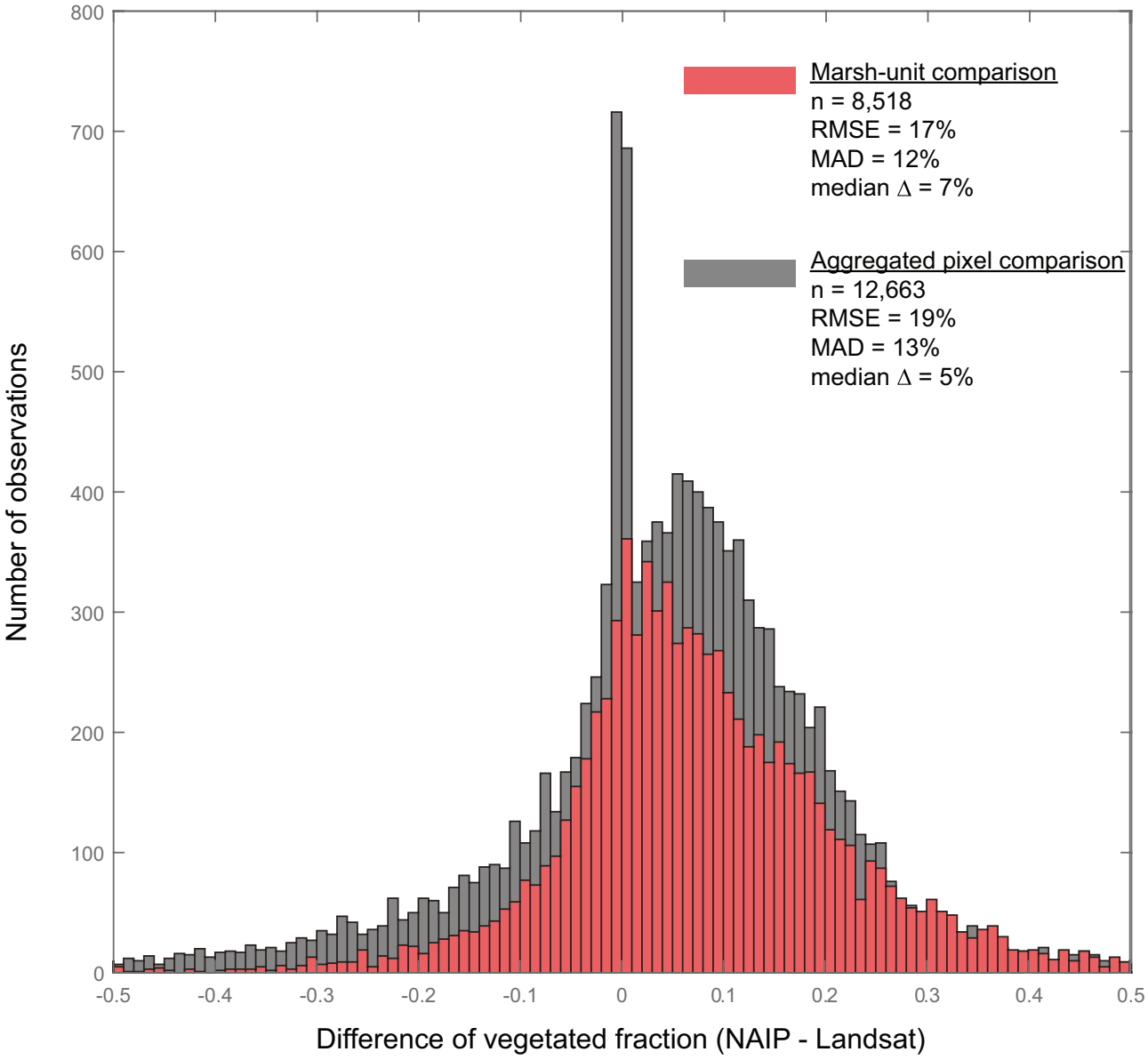


**Fig. 3** Comparison of US Department of Agriculture National Agriculture Imagery Program (NAIP) classification based vegetated fraction and Landsat-based estimate. Marsh-unit comparison aggregates NAIP and Landsat pixels over topographically constrained units; aggregated pixel comparison aggregates NAIP pixels (0.6×0.6 m) over Landsat pixel footprint (30×30 m). Comparison is based on eastern Chesapeake Bay dataset (Ackerman et al. 2021). RMSE is root-mean-square error, MAD is mean absolute deviation

continuous spectral estimates at the pixel-scale in the "Resolution and Aggregation Scales" section.

### Variogram Results in Specific Test Regions

The variogram was calculated annually for 5 years of data over 3.75 km × 3.75 km square areas (14 $km^2$), at five different locations on all three US coasts. The spatial autocorrelation of five test regions, quantified using the anisotropic variogram, demonstrates robust spatial patterns from year-to-year despite variability in the underlying UVVR values (Fig. 4). This indicates that the signal-to-noise ratio is high, and annual fluctuations in vegetative cover do not affect the underlying spatial pattern in the UVVR. Furthermore, the consistency of the variogram demonstrates that a 5-year average of the data will maintain spatial patterns and allow for a relative comparison of vegetative cover across marsh complexes. The largest deviation was observed in a single year (2017) at the Delta National Wildlife Refuge location, where a peak in spatial correlation at approximately 1 km resulted from increased UVVR values across the entire domain, perhaps due to anomalously high water levels during image collection. The shapes of the variograms also highlight the underlying variability in salt marsh morphology; e.g., the Sandwich Marsh location was characterized by two peaks, corresponding to the spacing of tidal channels. Variograms can help establish the annual consistency of the data, and to probe deeper aspects of salt marsh morphology. Applying the variogram over longer timescales as newer data become available may reveal underlying mechanisms of salt marsh loss (e.g., channel widening, pond expansion, submergence).

## Applications

The vegetative cover and UVVR datasets for the Atlantic, Gulf, and Pacific coasts of the conterminous USA are accessible through ScienceBase at https://doi.org/10.5066/P97DQXZP. Shapefiles are available for download, for annual data (2014–2018), the multi-year composite, and the standard deviation described above and used below in example applications. For web-based visualization of only the multi-year composite, users can visit the USGS Coastal Wetland Synthesis geonarrative at https://wim.usgs.gov/geonarrative/uscoastalwetlandsynthesis/.

### Multi-year Composite Aggregates at the Estuary and State Level

We exploited the national-scale data to compare marsh vegetation coverage and the UVVR at state and estuary scales to provide an example of how these data can be used for rapid assessment. Perhaps more importantly, this aggregation allows for up-to-date and efficient quantification and comparison of vegetated areas at spatial scales for which data are presently lacking. The wetland classification mask, based on the National Wetland Inventory (NWI), yields a total area but does not provide a dynamic differentiation between vegetated and unvegetated areas. We can therefore use the vegetated fraction estimates over the NWI mask to directly calculate total vegetated wetland area in each state and estuary. Ultimately, this estimate is necessary for tracking national-scale investments in restoration, carbon sequestration, habitat availability, and coastal protection.

We considered US state- and estuary-level aggregates along the three conterminous US coastlines. A state-level vegetated fraction was calculated as the mean of the aggregated pixels within each state and converted to a UVVR following Eq. (3). For estuary-level estimates, hydrological unit maps from the U.S. Geological Survey (USGS) Watershed Boundary Dataset (USGS 2013) were used to define the seaward and landward boundaries for each estuary (Supp. S1).

In practice, the Landsat-derived estimates will contain empty (null) values in completely unvegetated areas that exceed the pixel size (30 × 30 m). For example, a 60 m × 60 m pond within a salt marsh plain will be characterized by at least a single null value, and therefore not be included in an aggregated calculation of the vegetated fraction over that entire marsh complex. Similarly, highly fragmented wetland complexes with vast open-water areas but relatively small intact marsh plains may yield a misleadingly high estimate of vegetative cover due to large expanses of null values within the domain. Therefore, we present two estimates of the aggregated UVVR for state- and estuary-level estimates. First, a low-end estimate ($UVVR_{lo}$) is calculated by excluding all null values during aggregation, and a high-end estimate ($UVVR_{hi}$) is calculated by assuming all null cells are completely unvegetated and assigning a vegetative cover value of zero. For both estimates, a more restrictive mask was used that excluded a number of classes not generally representative of tidal wetlands (Supp. S2), and not considered germane to a state/estuary level comparison. Because this mask includes unvegetated classes (barrier islands, intertidal flats) that vary based on geomorphic environment or state-specific delineation, comparisons of $UVVR_{hi}$ between states and estuaries should be interpreted with caution. The primary role of this more restrictive mask is to yield a robust estimate of vegetated area for each region without inadvertently excluding potential vegetated areas.

#### State-Level Estimates

We analyzed the intra-annual mean vegetative cover and UVVR in the 22 CONUS coastal states (Table 1, Fig. 5). Louisiana and Florida account for over half of the nation's

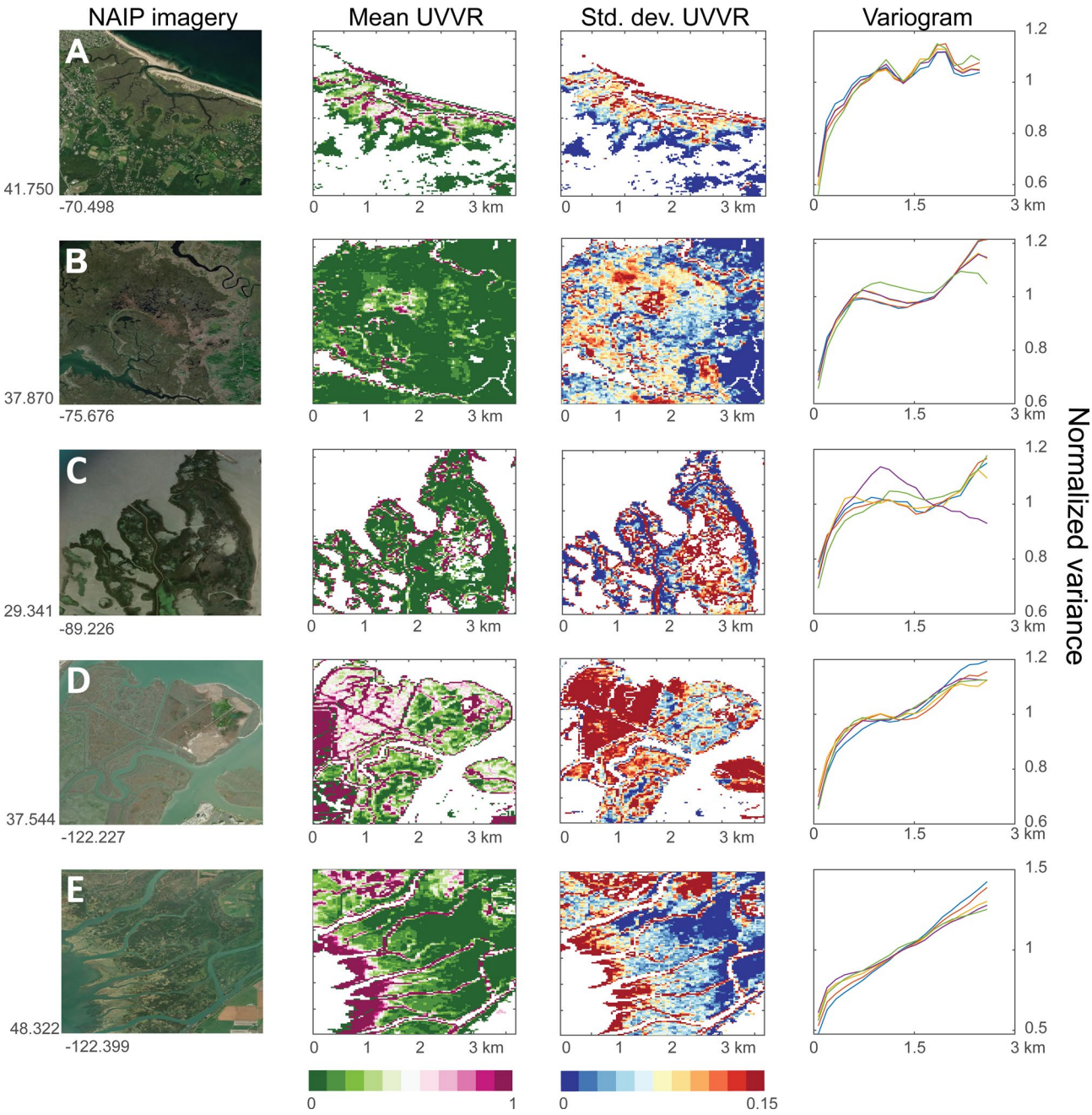


**Fig. 4** Aerial imagery, mean UVVR, standard deviation of UVVR values from five years, and spatial autocorrelation for each year of UVVR data (variogram), at five salt marsh complexes: **A**) Sandwich Marsh, MA; **B**) Saxis Wildlife Management Area, VA; **C**) Delta National Wildlife Refuge, LA; **D**) Bair Island, CA; and **E**) Skagit River Delta, WA. Each analysis area is 125×125 pixels, or 3.75×3.75 km. Annual variograms were normalized by mean variance to enable comparison of spatial autocorrelation. Similarity in variograms between years implies consistent spatial patterns between years

vegetated wetland area. Louisiana's wetlands, nearly continuous along the state's coast, account for 32% of the nation's total while Florida's wetlands, which include large expanses of mangrove in the southern portions of the state, represent 25% of the nation's total. Both states have relatively low $UVVR_{lo}$ indicating well-vegetated, intact wetland areas. However, Louisiana has a large $UVVR_{hi}$ due to fragmentation on spatial scales larger than the 30-m pixels.

South Carolina and Georgia each account for about 7% of the nation's total vegetated area, but both exhibit a high UVVR that is not connected with fragmentation or

**Table 1** Compilation of aggregated state level total wetland area, $UVVR_{lo}$ (null pixels excluded), $UVVR_{hi}$ (null pixels included as unvegetated), mean vegetated fraction over wetland mask, vegetated area, and percent of national total

| State | Total area ($km^2$) | $UVVR_{lo}$ | $UVVR_{hi}$ | Vegetated fraction | Vegetated area ($km^2$) | % of total |
|---|---|---|---|---|---|---|
| Louisiana | 6843 | 0.10 | 0.31 | 0.76 | 5228 | 32.1% |
| Florida | 4607 | 0.08 | 0.12 | 0.89 | 4113 | 25.3% |
| South Carolina | 1911 | 0.52 | 0.58 | 0.63 | 1213 | 7.5% |
| Georgia | 1640 | 0.46 | 0.49 | 0.67 | 1099 | 6.8% |
| Texas | 1151 | 0.22 | 0.28 | 0.78 | 898 | 5.5% |
| North Carolina | 992 | 0.14 | 0.18 | 0.85 | 842 | 5.2% |
| Maryland | 850 | 0.18 | 0.24 | 0.80 | 684 | 4.2% |
| New Jersey | 772 | 0.24 | 0.30 | 0.77 | 593 | 3.6% |
| Virginia | 811 | 0.33 | 0.50 | 0.67 | 542 | 3.3% |
| Delaware | 278 | 0.16 | 0.21 | 0.83 | 230 | 1.4% |
| Mississippi | 246 | 0.09 | 0.13 | 0.89 | 218 | 1.3% |
| Massachusetts | 154 | 0.13 | 0.27 | 0.79 | 122 | 0.7% |
| Washington | 136 | 0.23 | 0.31 | 0.76 | 104 | 0.6% |
| Oregon | 100 | 0.10 | 0.16 | 0.86 | 86 | 0.5% |
| Alabama | 96 | 0.10 | 0.14 | 0.88 | 84 | 0.5% |
| Maine | 90 | 0.10 | 0.25 | 0.80 | 72 | 0.4% |
| New York | 95 | 0.41 | 0.62 | 0.62 | 59 | 0.4% |
| California | 61 | 0.22 | 0.38 | 0.73 | 44 | 0.3% |
| Connecticut | 39 | 0.25 | 0.47 | 0.68 | 27 | 0.2% |
| New Hampshire | 20 | 0.13 | 0.26 | 0.79 | 16 | 0.1% |
| Rhode Island | 9 | 0.27 | 0.61 | 0.62 | 6 | 0.0% |
| Pennsylvania | 2 | 0.15 | 0.29 | 0.77 | 2 | 0.0% |
| Total | 20903 | NA | NA | NA | 16,281 | 100% |

open-water expansion. Closer inspection of aerial imagery and ground photos (Fig. 6) shows that sparseness of the vegetated plain and exposed sediment lead to relatively low estimates of vegetative cover. Satellite-based methods that use within-pixel, continuous spectral information to quantify vegetative cover account for sparseness of stems; this contrasts with visual classification methods that select a binary choice for a pixel (e.g., the NAIP-based methods described in the "Validation and Assessment with Aerial Imagery-Based Classification" section). In this particular case, visual classification of the plain in Fig. 6 would result in a "vegetated" selection, while the spectral estimate would assign a relatively low value of vegetative cover. We discuss these nuances in the "Resolution and Aggregation Scales" section.

The $UVVR_{lo}$ metric quantifies wetland plain integrity but neglects large open-water areas. The states with the lowest $UVVR_{lo}$, in addition to Louisiana and Florida as discussed above, are Mississippi, Oregon, Alabama, Maine, Massachusetts, and New Hampshire. The highest $UVVR_{lo}$ outside South Carolina and Georgia is found in New York and Virginia. In the case of New York, extensive ditching and the relatively small scales of the wetland complexes (which results in inclusion of open water within pixels) yield a low vegetative fraction and high UVVR. Much of Virginia's wetland area is contained within the Virginia Coastal Reserve, which has expansive intertidal flats as well as a dynamic coastline. In both New York and Virginia, barrier islands that are included in the wetland mask may account for low vegetative fraction as they may include bare sediment within back-barrier wetland pixels.

The $UVVR_{hi}$ metric is more difficult to interpret because it includes a number of NWI classes that will vary based on how those classification boundaries are drawn within each state. We include those classes in order to cover the largest possible area for vegetated area computations, but the metric may represent an underlying geomorphic characteristic in some cases. For example, in Louisiana, the large difference between $UVVR_{lo}$ and $UVVR_{hi}$ is due to marsh fragmentation, at scales larger than the 30-m pixel, which then generates empty values over the masked area. Conversely, the similarity between $UVVR_{hi}$ and $UVVR_{lo}$, as in South Carolina and Georgia, indicates intact marsh plain expanses, with little fragmentation despite sparsely vegetated plains. For tracking basin-scale changes, however, $UVVR_{hi}$ may be more useful for temporal trends as it can be scaled up into larger units and capture fragmentation changes.

### Estuary-Level Estimates

A total of 29 estuaries of varying size from 0.4 to over 1,200 $km^2$ were analyzed (Table 2, Fig. 7, Supp. S1). Chesapeake

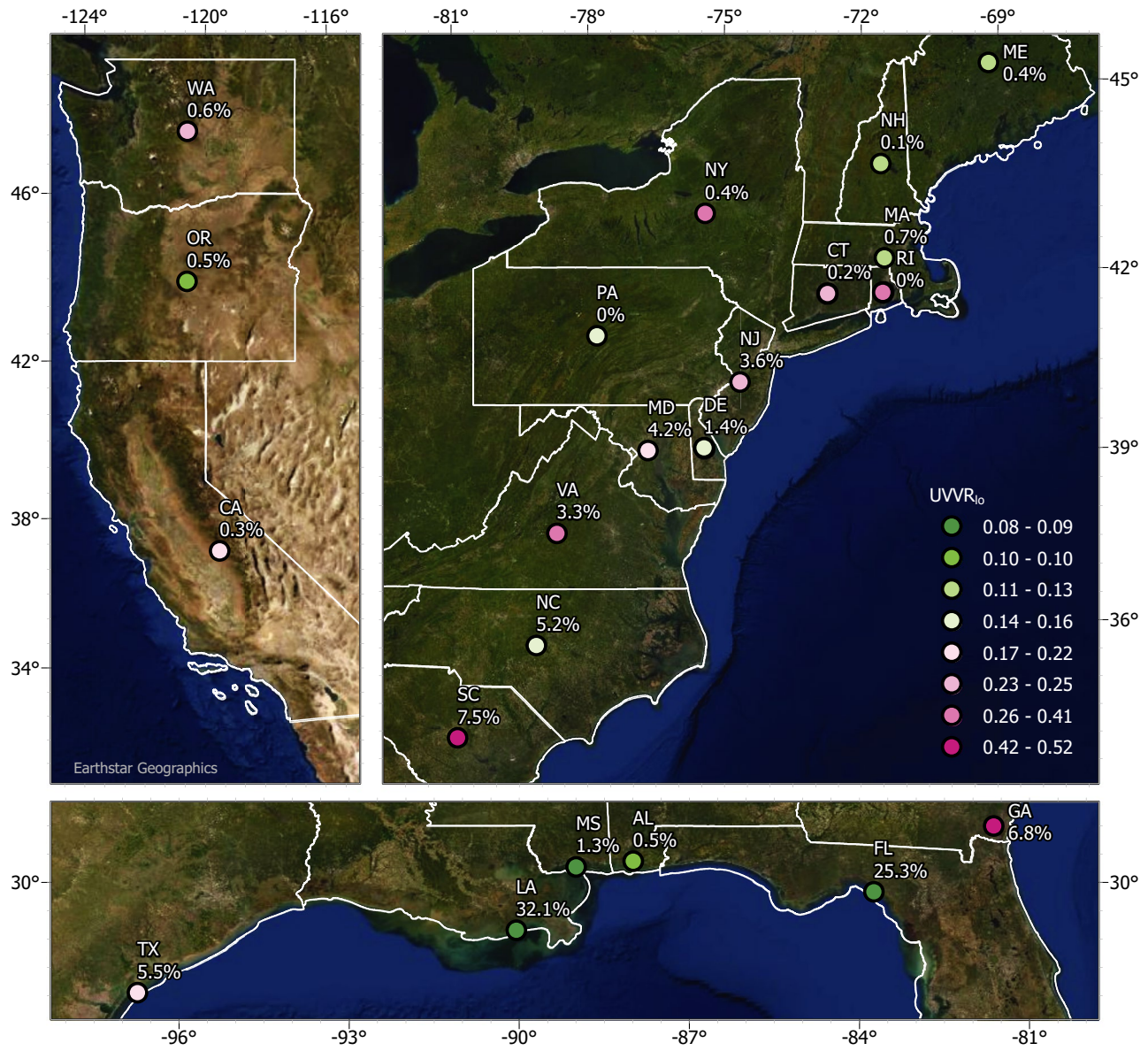


**Fig. 5** State-level UVVR$_{lo}$ (colored circles) and percent of national wetland area total (adjacent to state abbreviation). Basemap layer credits: VITA, Esri, HERE, Garmin, FAO, NOAA, EPA, USGS

Bay contains over 6% of the nation's vegetated wetland area, while the aggregate of the selected Louisiana coastal systems (Terrebonne Bay, Barataria Bay, Atchafalaya/Wax Lake Delta, Plaquemines-Balize Delta) accounts for over 8%. Albemarle/Pamlico Sounds and Delaware Bay were the next largest vegetated areas, with 5% and 3%, respectively. From a UVVR perspective, the detailed inventories mirror results at the state level. For example, the relatively large differences between UVVR$_{lo}$ and UVVR$_{hi}$ for Barataria Bay, Terrebonne Bay, and the Plaquemines-Balize Delta result from large open-water areas and fragmentation between relatively intact marsh plains (at the sub-30-m pixel scale). St. Helena Sound in South Carolina has a high UVVR$_{lo}$ and UVVR$_{hi}$ despite expansive marsh and little marsh fragmentation. This is due to the sparse vegetation signal over the vegetated plain (discussed above). Future research can connect the UVVR in such systems with stem density measurements and/or aboveground biomass, and regionally variable endmembers for calibration may be implemented if warranted. In the northeast, Long Island Sound and Narrangansett Bay, which cover portions of New York and Connecticut, show a large difference between UVVR$_{hi}$ and UVVR$_{lo}$, due to the small wetland plains relative to pixel size (which will naturally incorporate more open water/flats), as well as occurrence of constructed ditches and ensuing pool formation (Smith et al. 2021).


**Fig. 6** An in situ example of typical vegetative cover observed in South Carolina and Georgia salt marshes. Cross-marsh view (**A**) and a birds-eye view (**B**) for a marsh complex southeast of Charleston, SC (latitude: 32.7490334, longitude: -79.8985239), from April 6, 2021. (Photographs courtesy of Katie Luciano, South Carolina Department of Natural Resources)

Comparisons between estuaries and linkages with broad-scale external forcings are confounded by the myriad factors contributing to salt marsh degradation. The estuary-wide metrics are presented here to establish a baseline condition and enable tracking of vegetated habitat status through time for each specific system. As Wasson et al. (2019) pointed out, there are multiple factors contributing to marsh degradation that do not necessarily act consistently across all marsh environments. It is more appropriate to compare UVVR over time for marsh complexes within a similar setting, and therefore, we demonstrate methods to establish relative vulnerability within an estuary or marsh complex in the "Using the Composite and Standard Deviation for Vulnerability Assessment" section.

## Detecting Spatiotemporal Trends due to Restoration, Recovery, and Loss

Despite annual variability in the UVVR due to natural processes or artifacts, the data can be used to track restoration, recovery, and/or loss in areas with known histories. For example, techniques such as sediment placement and hydrologic restoration can be objectively judged based on the trajectory of the UVVR and vegetated fraction. While very high-resolution methods, such as unoccupied aerial systems imagery, can be performed over small spatial scales (and repeated often), the ability to track multiple regions with a single data set is efficient and standardizes processes across agencies and initiatives.

At Prime Hook National Wildlife Refuge in Delaware, extensive restoration of tidal hydrodynamic processes and seeding (U.S. Fish and Wildlife Service 2022b) led to increased vegetation in multiple regions, especially at the southeastern edge and central landward portion of the marsh (Fig. 8A). In Louisiana, sediment placement was performed in two bayous (Bayou Chevee and Turtle Bayou; USACE 2022) to restore open water to marsh. The annual data from 2014 to 2016 show unvegetated plains initially, followed by bare sediment, both with vegetation fractions of zero, with revegetation occurring over both areas by 2018 (Fig. 8B). In south San Francisco Bay, California, the Alviso–Island Ponds project breached salt pond levees in 2006 (California Wetlands Monitoring Workgroup 2022); restoration of tidal flows has accelerated marsh development at areas near the breach (Fig. 8C). Lastly, loss of vegetation due to storms can also be detected in impacted areas. In 2017, Hurricane Irma reduced the coverage of mangroves throughout South Florida through storm surge and ponding (Lagomasino et al. 2021); in Everglades National Park, the decrease in vegetative cover is readily detectable in 2018 (Fig. 8D).

## Using the Composite and Standard Deviation for Vulnerability Assessment

The annual variability in the UVVR can be deployed as a diagnostic tool for identifying vulnerable areas. Prior work has shown a stability threshold ~ 0.15, indicating that marshes with UVVRs above this threshold are more vulnerable to runaway expansion and conversion to open water (Wasson et al. 2019). Using this value as a 5-year composited UVVR and the standard deviation (sd) threshold, we can separate domains into four categories: stable with low uncertainty (mean and sd of UVVR < 0.15), unstable with low uncertainty (mean > 0.15 and sd < 0.15), unstable with high uncertainty (mean and sd of UVVR > 0.15), and stable with high uncertainty (mean

**Table 2** Compilation of aggregated estuary level total wetland area, $UVVR_{lo}$ (null pixels excluded), $UVVR_{hi}$ (null pixels included as unvegetated), mean vegetated fraction over wetland mask, vegetated area, and percent of national vegetated wetland area total. See Supp. S1 for list of hydrologic units used for each domain

| Name of domain | State | Total area ($km^2$) | $UVVR_{lo}$ | $UVVR_{hi}$ | Vegetated fraction | Vegetated area ($km^2$) | % of total |
|---|---|---|---|---|---|---|---|
| Chesapeake Bay | DE, MD, VA | 1266 | 0.17 | 0.25 | 0.80 | 1014 | 6.2% |
| Albemarle and Pamlico Sounds | NC, VA | 874 | 0.06 | 0.08 | 0.93 | 809 | 5.0% |
| Delaware Bay | NJ, PA, DE | 593 | 0.19 | 0.23 | 0.81 | 481 | 3.0% |
| Barataria Bay | LA | 689 | 0.12 | 0.50 | 0.67 | 459 | 2.8% |
| Terrebonne Bay | LA | 695 | 0.25 | 0.74 | 0.57 | 399 | 2.4% |
| Wax Lake Delta, Atchafalaya | LA | 344 | 0.01 | 0.08 | 0.93 | 319 | 2.0% |
| St. Helena Sound | SC | 458 | 0.61 | 0.68 | 0.59 | 272 | 1.7% |
| Timucuan Preserve | FL | 236 | 0.26 | 0.32 | 0.76 | 179 | 1.1% |
| Plaquemines-Balize Delta | LA | 204 | 0.11 | 0.36 | 0.74 | 150 | 0.9% |
| Ossabaw Sound | GA | 211 | 0.41 | 0.43 | 0.70 | 147 | 0.9% |
| Mississippi Sound | MS | 173 | 0.11 | 0.19 | 0.84 | 146 | 0.9% |
| Barnegat and Great Bays | NJ | 181 | 0.22 | 0.29 | 0.77 | 140 | 0.9% |
| San Francisco Bay | CA | 162 | 0.19 | 0.32 | 0.76 | 123 | 0.8% |
| Galveston Bay | TX | 122 | 0.21 | 0.29 | 0.78 | 95 | 0.6% |
| DE/MD/VA Coastal Bays | DE, MD, VA | 130 | 0.33 | 0.45 | 0.69 | 90 | 0.5% |
| Columbia River | OR | 86 | 0.10 | 0.16 | 0.86 | 74 | 0.5% |
| Mobile Bay | AL | 55 | 0.09 | 0.12 | 0.89 | 49 | 0.3% |
| Plum Island Sound | MA | 39 | 0.07 | 0.09 | 0.92 | 36 | 0.2% |
| Long Island Sound | CT, NY | 46 | 0.29 | 0.54 | 0.65 | 30 | 0.2% |
| Willapa Bay | WA | 35 | 0.23 | 0.28 | 0.78 | 27 | 0.2% |
| Puget Sound | WA | 33 | 0.36 | 0.55 | 0.65 | 21 | 0.1% |
| Hampton-Seabrook Complex | NH, MA | 16 | 0.16 | 0.27 | 0.79 | 13 | 0.1% |
| Wells/Rachel Carson NWRs | ME | 6.2 | 0.13 | 0.23 | 0.81 | 5.0 | < 0.1% |
| Narragansett Bay | RI, MA | 6.9 | 0.20 | 0.47 | 0.68 | 4.7 | < 0.1% |
| Elkhorn/Moro/Cojo Sloughs | CA | 3.5 | 0.43 | 0.58 | 0.63 | 2.2 | < 0.1% |
| Humboldt and Arcata Bays | CA | 2.9 | 0.48 | 0.68 | 0.59 | 1.7 | < 0.1% |
| Tijuana River Estuary | CA | 1.9 | 0.28 | 0.35 | 0.74 | 1.4 | < 0.1% |
| Tomales Bay | CA | 1.3 | 0.35 | 0.86 | 0.54 | 0.7 | < 0.1% |
| South Slough | OR | 0.4 | 0.24 | 0.42 | 0.71 | 0.3 | < 0.1% |

UVVR < 0.15 and sd > 0.15). The first two categories are the most informative, indicating areas with present-day stability or instability (and low uncertainty). The third category, unstable with high uncertainty, indicates large annual fluctuations over areas which are already over the stability threshold. This may be due to variable inundation (either from natural tidal processes or anthropogenic impoundment management), vegetation changes, or land management (e.g., controlled burn). Lastly, the fourth category, stable with high uncertainty, may result from the same aforementioned processes, though the variability is perhaps observed less frequently (e.g., episodic overwash of sand on back-barrier marshes).

As an example of this, we apply the categorization to Mackay Island National Wildlife Refuge, in northern Currituck Sound, North Carolina. The categorization, with thresholds at 0.15, isolates the four aforementioned regions, which can then be mapped (Fig. 9). Most of the complex (71%) falls within the first category of stability with low uncertainty, while 13% falls within the unstable and low uncertainty category. These areas mostly correspond to the northern region of the island where there are large open-water ponds and fragmented marsh plain. Two managed impoundments, on the southern and western edges, account for most of the unstable with uncertainty category (14%), likely due to annual changes in water level that modulate the UVVR. Less than 2% of the complex presents as the final category. The value of this assessment is two-fold: it allows for rapid characterization of vulnerability over large spatial scales, with an objective metric used to categorize areas. Secondly, the relative distribution of these categories can be observed through time with updated products, allowing for a tracking of vulnerability, again with an objective and reproducible metric.

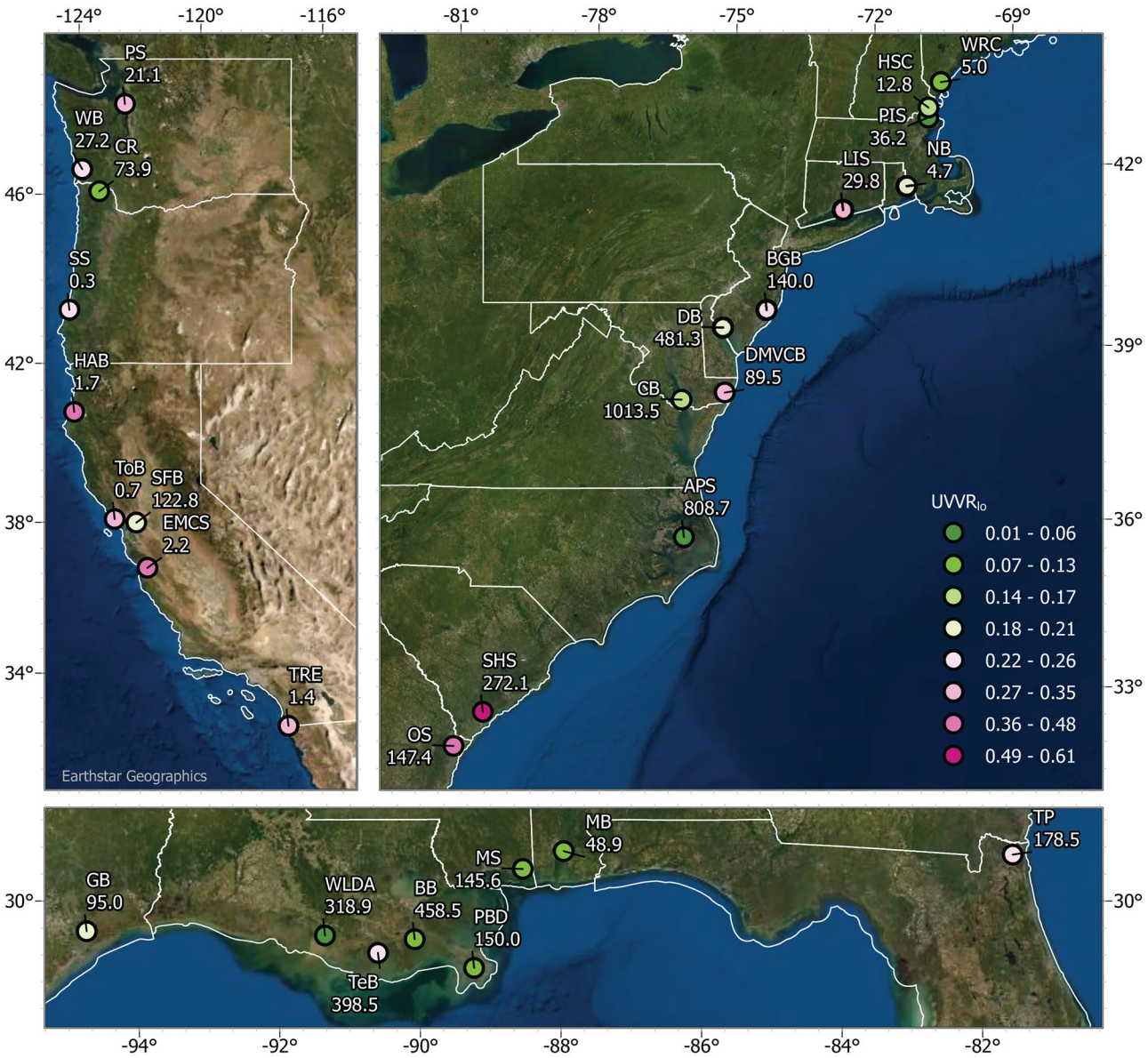


**Fig. 7** Estuary-level UVVR$_{lo}$ (colored circles) and vegetated area (in km$^2$, adjacent to estuary identifier). Basemap layer credits: VITA, Esri, HERE, Garmin, FAO, NOAA, EPA, USGS. See Supplemental S2 for details

## Discussion

The development of a national inventory of wetland vegetative cover and UVVR provides a baseline data set for tracking trends in salt marsh trajectory across state, estuary, and system scales. We also demonstrate the use of the UVVR for spatial assessment of vulnerability across the marsh complex scale, where targeted management and restoration decisions are typically made. These data are ultimately most valuable when used at the appropriate scale, in combination with other relevant metrics (e.g., elevation, tide range, aboveground biomass, habitat usage). Below, we discuss the impact of resolution on interpretation of wetland processes and highlight the value of these data for national-scale efforts.

### Resolution and Aggregation Scales

The spatiotemporal completeness of coverage and resolution of satellite imagery together with modern computational capabilities (i.e., cloud-based solutions) makes satellite imagery an ideal dataset for analyses at national and regional scales. For this reason, we used Landsat imagery for exploring spatial trends at the national scale, compared state-level UVVR aggregates, and provided results at estuary-level scales. Improvements could include non-linear methods of

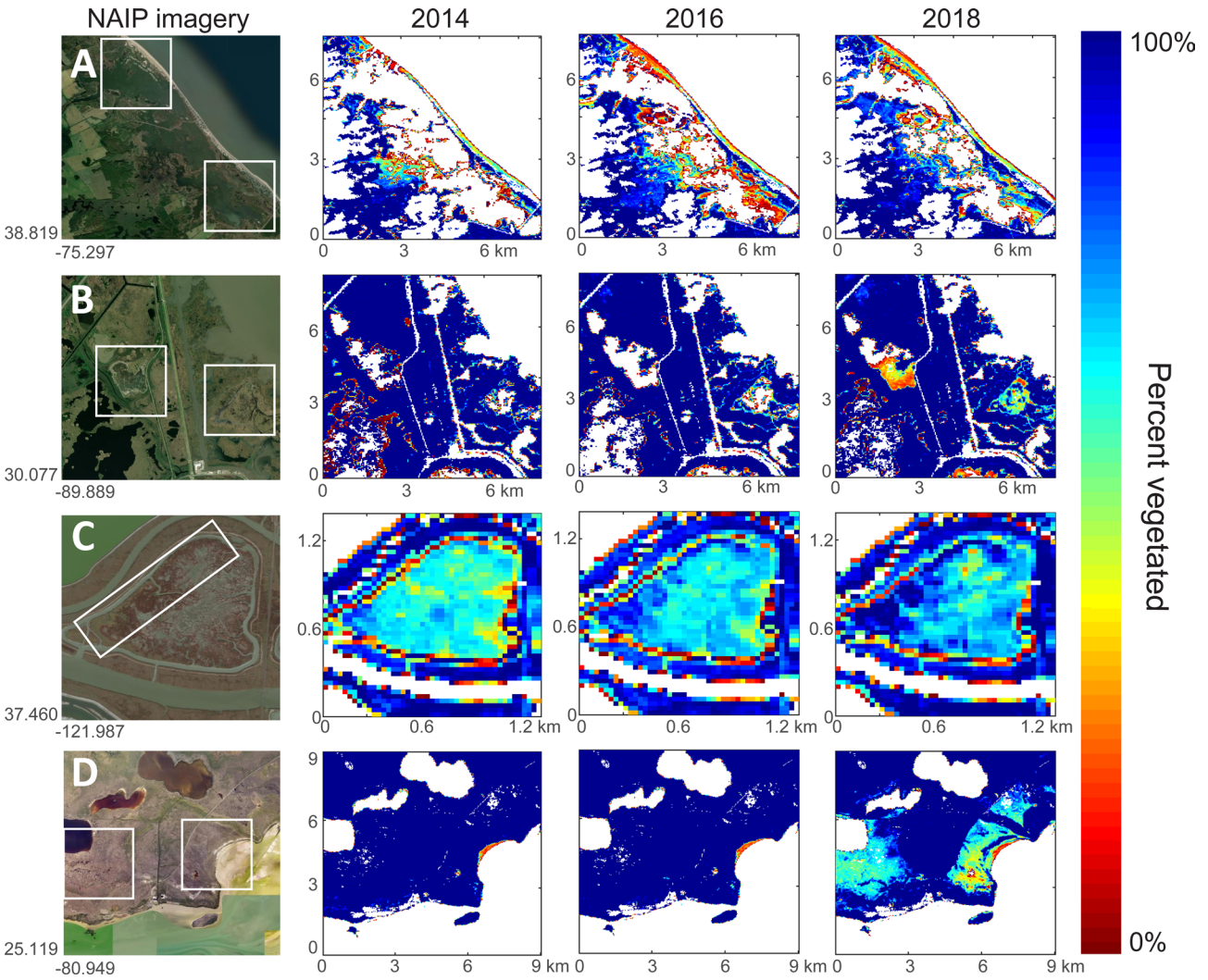


**Fig. 8** Aerial imagery and annual vegetative cover at **A**) Prime Hook NWR, DE; **B**) Bayou Sauvage NWR, LA; **C**) Don Edwards San Francisco Bay NWR; and **D**) Everglades National Park, FL. White boxes over NAIP imagery indicate areas of largest vegetative change. Panels A–C represent changes due to tidal restoration, sediment placement, and levee breaching respectively; Panel D represents dieback due to Hurricane Irma in 2017

spectral unmixing, regionally variable endmembers, and other methods of image compositing and/or analysis such as harmonic analysis.

However, for analyses at smaller scales (investigating variations within an estuary or a marsh complex), using higher-resolution data, such as sub-1-m resolution NAIP imagery, and delineating the study area into marsh units to calculate aggregates (Defne et al. 2020; Ganju et al. 2020) would enhance fidelity. Either of the pixel-based or marsh unit approaches are suitable for geospatial analysis to explore trends in wetland status, but a mixed use of methods or a direct comparison between results from different methods for deriving conclusions could be misinterpreted due to differences in spatial resolution and spectral resolution of source data. For example, imagery with sub-meter resolution can directly capture creeks narrower than 10 m or resolve narrow swaths of vegetation (i.e., < 30 m), whereas these features are assimilated in the fractional proportion of cover type for the Landsat-based approach.

The UVVR concept was originally developed using supervised classification of aerial imagery (Defne et al. 2020), where individual pixels are classified as vegetated or unvegetated, based on four-band imagery and elevation. The classification therefore imposes a binary choice on each pixel and does not account for sparseness of vegetation. In other words, a sparsely vegetated mudflat may be identified as unvegetated, though it technically contains a low density of stems. In contrast, satellite-based methods that are based on spectral returns will identify a sparsely vegetated pixel

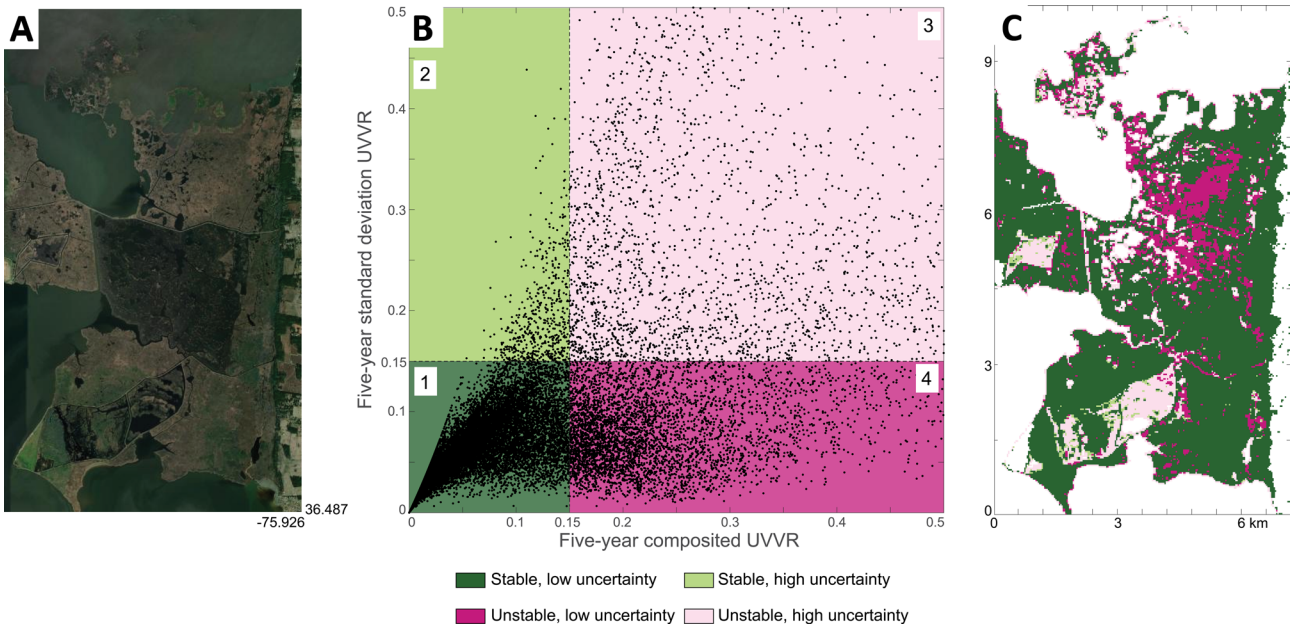


**Fig. 9** Application of UVVR threshold analysis at Mackay Island National Wildlife Refuge, North Carolina, USA. **A**) aerial image of the region (USDA 2022). **B**) scatterplot of five-year composited and standard deviation of UVVR, used to identify areas that have crossed the nominal 0.15 stability threshold; 1) indicates stable, low uncertainty pixels; 2) indicates stable, high uncertainty pixels; 3) indicates unstable, high uncertainty pixels; and 4) indicates unstable, low uncertainty pixels. **C**) mapping of four stability regions

with a relative value (as opposed to a binary choice). Ultimately, the spectral signal is fundamentally related to aboveground biomass which is in turn related to vegetative cover over some larger areal unit. Therefore, the interpretation of vegetative cover and UVVR should be based on the use of the data. For tracking the distribution of channels, flats, and plains using the UVVR, the visual, supervised classification method is likely the most robust. However, if the density of vegetation within the plain is of interest (for computations of wave attenuation, carbon stock, habitat suitability), then a continuous within-pixel estimate may be more relevant. In both cases, data must be aggregated over some spatial scale, as the relevance of vegetative cover becomes questionable as the footprint area approaches zero. Though not attempted here, there is also the option of within-pixel vegetative cover estimates (not binary) using aerial imagery. However, given the variability in aerial imagery based on sensor platforms, this may result in variable calibration across flight paths. The inconsistency in spectral information contained within the NAIP imagery leads to errors in its ability to estimate percent cover. It is also important to note that the Landsat imagery is collected more frequently than NAIP imagery (2–3 years return period). Finally, geo-rectification errors may lead to some differences in the ground area covered by the NAIP- and Landsat-derived percent cover estimates, which may lead to further discrepancy between the two datasets and explain some of the inaccuracy. Ultimately, supervised classification methods allow for flexibility in assessing imagery before and after processing (e.g., to account for seasonal differences), but include some subjectivity in the classification and interpretation of the results. As high-resolution commercial satellite imagery products increase in availability and temporal resolution, the creation of cloud-free composites with improved spectral consistency as compared to aerial imagery may become increasingly possible. This may enable the creation of high-resolution vegetated cover estimates from these products.

## Value of a Nationally Consistent Data Set

Multiple federal, state, and local agencies, as well as land conservation groups, are focused on coastal wetland management and restoration, with different objectives. A consistent national UVVR and vegetated fraction dataset provide a critical baseline for rapid assessment of wetland status for multiple agencies and objectives simultaneously. For example, the U.S. Fish and Wildlife Service is primarily concerned with habitat restoration for endangered species that use vegetated areas of salt marshes across the entire nation. Our study enables quantification of vegetated area at every coastal refuge and a baseline dataset for tracking future restoration efforts. On a national basis, CONUS-wide carbon inventories that include coastal wetlands could integrate vegetative cover estimates, while forecasts will benefit from wetland stability predictions that can be based on the UVVR. For states and local agencies, the UVVR at 30-m

resolution can be used in conjunction with finer-scale mapping efforts once vulnerable areas are identified. Updating satellite-based wetland metrics for entire periods-of-record and refining them with high-resolution sensors will be important for furthering management and research objectives. However, Landsat 5 may be used also to extend the analyses from 1984 to 2012.

## Conclusions

In this study, we presented a method to estimate vegetative cover and associated metrics for coastal wetlands of the conterminous United States. This dataset enables the observation of outcomes of multiple processes of interest across tidal wetlands. These data can be used to establish baseline vegetative cover at estuary and state scales, and to track annual changes in vegetation due to restoration or loss. Aggregation across estuary and state scales provides contrasting estimates of the UVVR depending on the inclusion of open-water areas often indicative of lateral instability. At the individual estuary scale, the annual variability can be used to classify vulnerable areas using threshold values for the UVVR. In contrast to field-based methods, remote sensing offers an objective technique to track wetland trajectory in response to storms, sea-level rise, and anthropogenic actions. As higher-resolution sensors and approaches become available, remote sensing will be an important tool in coastal wetland research and management across smaller scales. Furthermore, the data offer an opportunity for developing and testing models of wetland geomorphology, and improving our basic understanding of wetland response to complex biophysical factors.

**Acknowledgements** Landsat Spectral Indices products courtesy of the U.S. Geological Survey Earth Resources Observation and Science Center. Any use of trade, firm, or product names is for descriptive purposes only and does not imply endorsement by the US Government. Nicholas Enwright, Kathy Weber, and two anonymous reviewers provided helpful comments on the manuscript.

**Funding** This work was supported by the U.S. Geological Survey's Coastal and Marine Hazards/Resources Program.



## References

Ackerman, K.V., Z. Defne, and N.K. Ganju. 2021. Coastal wetlands of the Blackwater region, Chesapeake Bay, Maryland. *U.S. Geological Survey data release*, https://doi.org/10.5066/P9M7H6XG.

Barbier, E.B., S.D. Hacker, C. Kennedy, E.W. Koch, A.C. Stier, and B.R. Silliman. 2011. The value of estuarine and coastal ecosystem services. *Ecological Monographs* 81 (2): 169–193.

Burns, C.J., M. Alber, and C.R. Alexander. 2021. Historical changes in the vegetated area of salt marshes. *Estuaries and Coasts* 44 (1): 162–177.

Cahoon, D.R., J.C. Lynch, C.T. Roman, J.P. Schmit, and D.E. Skidds. 2019. Evaluating the relationship among wetland vertical development, elevation capital, sea-level rise, and tidal marsh sustainability. *Estuaries and Coasts* 42 (1): 1–15.

California Wetlands Monitoring Workgroup (CWMW). 2021. EcoAtlas. https://www.ecoatlas.org. Accessed January 11, 2022.

Couvillion, B.R., H.J. Beck, J. Dugas, A. Garber, and K. Mouton. 2018. Coastwide Reference Monitoring System (CRMS) 2005, 2008, 2012, and 2015 land-water matrices. *U.S. Geological Survey data release*, https://doi.org/10.5066/F75D8Q92.

Couvillion, B.R., H. Beck, D. Schoolmaster, and M. Fischer. 2017. Land area change in coastal Louisiana: 1932 to 2016. *U.S. Geological Survey Scientific Investigations Map* 3381, 16 p. pamphlet, https://doi.org/10.3133/sim3381.

Couvillion, B.R., N.K. Ganju, and Z. Defne. 2021. An Unvegetated to Vegetated Ratio (UVVR) for coastal wetlands of the Conterminous United States (2014–2018). *U.S. Geological Survey data release*, https://doi.org/10.5066/P97DQXZP.

Cowardin, L.M., V. Carter, F.C. Golet, and E.T. LaRoe. 1979. Classification of wetlands and deepwater habitats of the United States. U.S. Department of the Interior, Fish and Wildlife Service, Washington, D.C., pp. 131.

D'Alpaos, A., and M. Marani. 2016. Reading the signatures of biologic–geomorphic feedbacks in salt-marsh landscapes. *Advances in Water Resources* 93: 265–275.

Deegan, L.A., D.S. Johnson, R.S. Warren, B.J. Peterson, J.W. Fleeger, S. Fagherazzi, and W.M. Wollheim. 2012. Coastal eutrophication as a driver of salt marsh loss. *Nature* 490 (7420): 388–392.

Defne, Z., A.L. Aretxabaleta, N.K. Ganju, T.S. Kalra, D.K. Jones, and K.E. Smith. 2020. A geospatially resolved wetland vulnerability index: synthesis of physical drivers. *PloS one* 15(1): p.e0228504.

European Space Agency. 2022. Copernicus Sentinel-2 surface reflectance data (2015–2019). Accessed at: https://earthexplorer.usgs.gov/. (last date accessed: 5 April 2022).

Fagherazzi, S. 2013. The ephemeral life of a salt marsh. *Geology* 41 (8): 943–944.

Feagin, R.A., I. Forbrich, T.P. Huff, J.G. Barr, J. Ruiz-Plancarte, J.D. Fuentes, R.G. Najjar, R. Vargas, A. Vázquez-Lule, L. Windham-Myers, and K.D. Kroeger. 2020. Tidal wetland gross primary production across the continental United States, 2000–2019. *Global Biogeochemical Cycles*, 34 (2): p.e2019GB006349.

Ganju, N.K., Z. Defne, and S. Fagherazzi. 2020. Are elevation and open-water conversion of salt marshes connected? *Geophysical Research Letters*, 47 (3): p.e2019GL086703.

Ganju, N.K., Z. Defne, M.L. Kirwan, S. Fagherazzi, A. D'Alpaos, and L. Carniello. 2017. Spatially integrative metrics reveal hidden vulnerability of microtidal salt marshes. *Nature Communications* 8 (1): 1–7.

Kirwan, M.L., G.R. Guntenspergen, A. D'Alpaos, J.T. Morris, S.M. Mudd, and S. Temmerman. 2010. Limits on the adaptability of coastal marshes to rising sea level. *Geophysical research letters* 37 (23).

Kriegler, F.J., W.A. Malila, R.F. Nalepka, and W. Richardson. 1969. Preprocessing transformations and their effect on multispectral recognition. *Remote Sensing of the Environment* 6: 97–132.

Lagomasino, D., T. Fatoyinbo, E. Castañeda-Moya, B.D. Cook, P.M. Montesano, C.S. Neigh, L.A. Corp, L.E. Ott, S. Chavez, and D.C. Morton. 2021. Storm surge and ponding explain mangrove dieback in southwest Florida following Hurricane Irma. *Nature Communications* 12 (1): 1–8.

Leonardi, N., I. Carnacina, C. Donatelli, N.K. Ganju, A.J. Plater, M. Schuerch, and S. Temmerman. 2018. Dynamic interactions between coastal storms and salt marshes: A review. *Geomorphology* 301: 92–107.

Mariotti, G. 2020. Beyond marsh drowning: the many faces of marsh loss (and gain). *Advances in Water Resources* 144: 103710.

National Oceanic and Atmospheric Administration (NOAA). 2022. Coastal change analysis program (C-CAP) regional land cover. NOAA Office for Coastal Management. www.coast.noaa.gov/htdata/raster1/landcover/bulkdownload/30m_lc/. Accessed January 11, 2022.

Neckles, H.A., G.R. Guntenspergen, W.G. Shriver, N.P. Danz, W.A. Wiest, J.L. Nagel, and J.H. Olker. 2013. Identification of metrics to monitor salt marsh integrity on National Wildlife Refuges in relation to conservation and management objectives. USGS Patuxent Wildlife Research Center, Laurel, Maryland. pp. 226. https://www.pwrc.usgs.gov/prodabs/pubpdfs/7828_Neckles.pdf. Accessed January 11, 2022.

Rangoonwala, A., N.M. Enwright, E. Ramsey III., and J.P. Spruce. 2016. Radar and optical mapping of surge persistence and marsh dieback along the New Jersey Mid-Atlantic coast after Hurricane Sandy. *International Journal of Remote Sensing* 37 (7): 1692–1713.

Redfield, A.C. 1972. Development of a New England salt marsh. *Ecological Monographs* 42 (2): 201–237.

Schwanghart, W. 2021. Experimental (semi-) variogram, MATLAB central file exchange. (https://www.mathworks.com/matlabcentral/fileexchange/20355-experimental-semi-variogram). Accessed March 24, 2021.

Smith, J.A., S.C. Adamowicz, G.M. Wilson, and I. Rochlin. 2021. "Waffle" pools in ditched salt marshes: Assessment, potential causes, and management. *Wetlands Ecology and Management*. https://doi.org/10.1007/s11273-021-09835-3.

Sun, C., S. Fagherazzi, and Y. Liu. 2018. Classification mapping of salt marsh vegetation by flexible monthly NDVI time-series using Landsat imagery. *Estuarine, Coastal and Shelf Science* 213: 61–80.

U.S. Army Corps of Engineers. 2022. Lake Pontchartrain and Vicinity HSDRRS Mitigation. Accessed at: https://www.mvn.usace.army.mil/Missions/Environmental/NEPA-Compliance-Documents/HSDRRS-Projects/PIER-36-Bayou-Sauvage-Turtle-Bayou-and-New-Zydeco-Ridge-Restoration/ . (last date accessed: 6 April 2022)

U.S. Department of Agriculture. 2022. National Agriculture Imagery Program (NAIP) Georectified Digital Imagery. Accessed at: https://earthexplorer.usgs.gov/. (last date accessed: 5 April 2022). https://doi.org/10.5066/F7QN651G

U.S. Fish and Wildlife Service (USFWS). 2022a. National wetland inventory wetland classification codes. https://www.fws.gov/wetlands/data/wetland-codes.html. Accessed 11 Jan 2022.

U.S. Fish and Wildlife Service (USFWS). 2022b. Prime Hook National Wildlife Refuge marsh restoration. https://www.fws.gov/refuge/Prime_Hook/what_we_do/marshrestoration.html. Accessed 11 Jan 2022.

U.S. Geological Survey (USGS). 2013. Federal standards and procedures for the national watershed boundary dataset (WBD). *US Geological Survey Techniques and Methods* pp. 11-A3.

U.S. Geological Survey (USGS). 2022a. USGS 3D Elevation Program Digital Elevation Model. https://elevation.nationalmap.gov/arcgis/rest/services/3DEPElevation/ImageServer. Accessed 11 Jan 2022.

U.S. Geological Survey (USGS). 2022b. Landsat SR-derived spectral indices pixel quality band. https://www.usgs.gov/landsat-missions/landsat-sr-derived-spectral-indices-pixel-quality-band. Accessed 11 Jan 2022.

Vermote, E., C. Justice, M. Claverie, and B. Franch. 2016. Preliminary analysis of the performance of the Landsat 8/OLI land surface reflectance product. *Remote Sensing of Environment* 185: 46–56.

Wasson, K., N.K. Ganju, Z. Defne, C. Endris, T. Elsey-Quirk, K.M. Thorne, C.M. Freeman, G. Guntenspergen, D.J. Nowacki, and K.B. Raposa. 2019. Understanding tidal marsh trajectories: evaluation of multiple indicators of marsh persistence. *Environmental Research Letters* 14 (12): 124073.

Wickham, J., S.V. Stehman, D.G. Sorenson, L. Gass, and J.A. Dewitz. 2021. Thematic accuracy assessment of the NLCD 2016 land cover for the conterminous United States. *Remote Sensing of Environment* 257: 112357.

Xu, H. 2006. Modification of normalised difference water index (NDWI) to enhance open water features in remotely sensed imagery. *International Journal of Remote Sensing* 27 (14): 3025–3033.

Zha, Y., J. Gao, and S. Ni. 2003. Use of normalized difference built-up index in automatically mapping urban areas from TM imagery. *International Journal of Remote Sensing* 24 (3): 583–594.